COMMUNICATION

Electric field gradient quadrupole Raman modes observed in plasmon-driven catalytic reactions revealed by HV-TERS

Zhenglong Zhang,[ab] Mengtao Sun,[*a] Panpan Ruan,[a] Hairong Zheng[b] and Hongxing Xu[ac]

Electric field gradient quadrupole Raman modes are observed in plasmon-driven chemical reactions investigated with high vacuum tip-enhanced Raman spectroscopy (HV-TERS). TER spectra reveal that 4-nitrobenzenethiol (4NBT) catalytically dimerizes to dimercaptoazobenzene (DMAB) under an HV-TERS setup. More importantly, we find that the electric field gradient leads to strong enhancement of the infrared (IR)-active modes of DMAB. The observation of both the Raman-active and IR-active modes of DMAB provides spectral evidence for ultrasensitive chemical analysis.
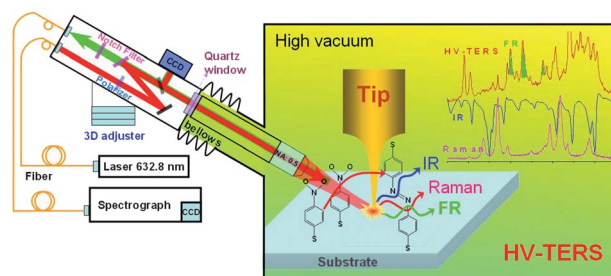
Plasmon chemistry is an emerging topic in nanophotonics.[1–10] It was found that hot electrons generated from plasmon decay play important roles in surface catalytic reactions.[8,9] Such reactions are referred to as plasmon-driven catalytic reactions. High vacuum tip-enhanced Raman spectroscopy (HV-TERS) is among the best candidates to study plasmon-driven catalytic reactions since it enables us to *in situ* monitor and control the reaction at specific catalytic sites with enormous surface sensitivity.[11,12] The dimerization of 4-nitrobenzenethiol (4NBT) to dimercaptoazobenzene (DMAB) is the most-studied plasmon-driven reaction.[9,10] The Raman-active modes of DMAB have been clearly observed and the experimental temperature has been estimated from ultrasensitive Stokes and anti-Stokes Raman spectra.[9]

In surface enhanced Raman spectroscopy (SERS)[13] and near field Raman spectroscopy,[14] it has been reported that the electric field gradient associated with a metal substrate enables both the molecular Raman- and infrared (IR)-active modes to be observed. Further, in linear HV-TERS, experimental observations of IR-active modes[15] and Fermi resonance[15,16] have been

reported. In nonlinear HV-TERS, Fermi resonance[16] and Darling–Denison[17,18] resonance have also been experimentally observed.[16,19]

In this communication, we utilized HV-TERS to study the plasmon-driven chemical reaction of DMAB dimerized from 4NBT adsorbed on the Au substrate. It was found that the electric field gradient effect results in strong enhancement of the IR-active modes of DMAB. Theoretical calculations were performed and agreed well with observations. The simultaneous observation of the Raman- and IR-active modes of DMAB in HV-TER spectra provides spectral evidence for ultrasensitive chemical analysis. The setup of HV-TERS, the chemical reaction, and vibrational spectra, including Raman and IR spectra, can be seen from Scheme 1.

Spectra were measured using a home-built HV-TERS setup.[9a] It consists of a home-built scanning tunneling microscope (STM) in a high vacuum chamber, a Raman spectrometer with a 100 μW 632.8 nm He–Ne laser incident at 60° to the tip axis, and piezo stages for three-dimensional tip and sample manipulations. The long working distance objective (NA = 0.5) was placed in the high vacuum chamber with a pressure of 10^{-7} Pa. The holographic grating (1800 grooves per mm) and the slit lead to a spectral resolution of 1 cm^{-1}. The tunneling current and bias voltage are 1 nA and 1 V respectively. A gold tip with a diameter of 50 nm was made by electrochemical etching from a

[a] Beijing National Laboratory for Condensed Matter Physics, Institute of Physics, Chinese Academy of Sciences, P. O. Box 603-146, Beijing, 100190, People's Republic of China. E-mail: mtsun@iphy.ac.cn

[b] College of Physics and Information Technology, Shaanxi Normal University, Xi'an, 710062, People's Republic of China

[c] School of Physics & Technology, Wuhan University, Wuhan, 430072, People's Republic of China

Scheme 1 The setup of HV-TERS, the chemical reaction, and vibrational spectra, including Raman and IR spectra.

0.25 mm diameter gold wire.[20] The gold substrate was prepared by evaporating a 100 nm metal film onto newly cleaned mica films under high vacuum. The Au films were then immersed in 1×10^{-5} M 4NBT and DMAB ethanol solutions for 24 hours successively and were further washed with ethanol for 10 minutes to ensure that there was only one monolayer of molecules adsorbed on the substrate. Samples were immediately put into the high vacuum chamber after preparation. In order to get a good signal-to-noise ratio, TERS signals excited at 632.8 nm were collected with an acquisition time of 40 seconds and each spectrum was the accumulation of 20 separate acquisitions. Normal Raman spectra (NRS) of 4NBT and DMAB powders were measured using Leica microscopy equipment in a confocal Raman spectroscopic system (Renishaw, Invia), where the illumination laser wavelength was 632.8 nm as well. The IR vibrational spectrum was performed using an Excalibur 3100.
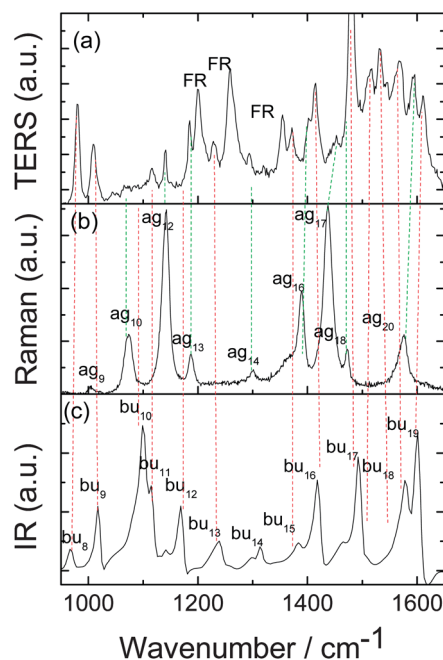
To evidence the dimerization reaction of 4NBT to DMAB, we compared the genetic NRS of 4NBT powder (Fig. 1(a)) to the TER spectrum of 4NBT adsorbed on the gold substrate after 5 μW laser power (5% of its full power) illumination (Fig. 1(b)). The observed strong Raman peak at 1336 cm^{-1} in Fig. 1(a) was from the –NO$_2$ stretching modes.[5,21] The same Raman features in these two spectra suggest that, at this low laser intensity, the plasmon intensity was below the energy threshold of the chemical reaction[9a] therefore the 4NBT molecules did not undergo dimerization. In contrast, when the laser was operated at its full power, the measured TER spectrum (Fig. 1(c)) shows a much higher number of Raman peaks, indicating there were 4NBT molecules dimerized to DMAB. It should be noted that the vibrational mode of 4NBT at 1336 cm^{-1} in Fig. 1(c) was weakened by the chemical reaction but it did not vanish completely.
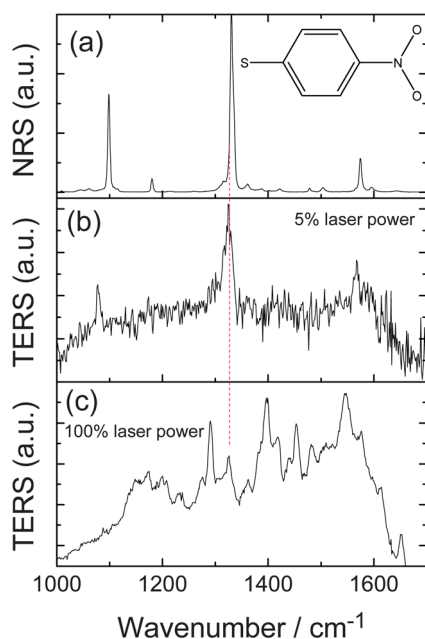
To support our conclusion that 4NBTs have dimerized to DMAB, we also measured the TER spectrum of DMAB adsorbed on a gold film (Fig. 2(a)) and the genetic NRS of DMAB powder (Fig. 2(b)). We also measured the IR vibrational spectrum (Fig. 2(c)). It could be observed that the two DMAB spectra were significantly different. Previous theoretical calculations[1,9a] revealed that these "additional peaks" in Fig. 2(a) were from the bu modes of DMAB. The calculations of ag and bu modes for Raman and IR spectra of DMAB are demonstrated in ref. 1. Therefore in the Au tip–Au substrate geometry, both the Raman- and the IR-active modes were simultaneously *in situ* observed. Further, comparing Fig. 2(b) to Fig. 2(a) in ref. 9a shows that the NRS of DMAB powder is almost the same as the TER spectrum of DMAB adsorbed on a silver film, indicating that the metal substrate material significantly affects the TER spectra. As will be discussed in the theory section, this observed substrate effect in HV-TERS comes from the electric field gradient effect. It should be noted that in Fig. 2(a) the ag$_{13}$, bu$_{13}$ and bu$_{15}$ peaks were splitted into two peaks. Our previous study revealed that the higher energy peak is due to the overtone mode[15] of Fermi resonance.[16] The Fermi resonance results in an overtone of different fundamental modes, or a combined mode appears in the vibrational spectra by gaining spectral weight from a fundamental mode.[16] Further, while SERS is a far field measurement in which the IR-active modes cannot be observed,[5] HV-TERS measures the near field, and the electric field gradient in near field strongly enhances the IR-active mode.[14,16]

To provide further evidence for the catalytic reaction, we directly compared the TER spectrum after full-intensity laser illumination (Fig. 1(c)) to the genetic TER spectrum of DMAB (Fig. 2(a)). The result is shown in Fig. 3. It was found that almost

Fig. 1 (a) Genetic normal Raman spectrum of 4NBT powders, (b) TER spectrum of the 4NBT adsorbed on a gold film at 5% laser power and (c) full laser power.

Fig. 2 (a) TER spectrum of DMAB adsorbed on a gold film, (b) the normal Raman spectrum of DMAB powder, and (c) the IR spectrum of DMAB.

all the peak positions match perfectly in the two TERS spectra, although the peak intensities are significantly different. The explanation of the intensity differences is that the reaction of 4NBT dimerizing to DMAB is not a complete reaction and therefore there were 4NBT molecules remaining in the sample when Fig. 1(c) was measured. The existence of 4NBT molecules can be proved by the presence of the 1336 cm^{-1} peak. In order to achieve complete reaction, a much stronger plasmon intensity is required, which is beyond the limitation of our experimental setup.

In order to analyze the experimental observations theoretically, we performed calculations to compute the charge distribution of DMAB molecules located between two metal surfaces using the DFT method, the PW91PW91 functional, the 6-31G (d) basis set for N, S, C, N and H, and the LANL2DZ basis set for Au and Ag using Gaussian 09 software.[22] For simplicity, Au$_5$–DMAB–Au$_5$ and Au$_5$–DMAB–Ag$_5$ were used to mimic the Au tip–Au/Au substrate and Au tip–Au/Ag substrate configurations, respectively. For the Au tip–Au substrate geometry, it was found that the charge density is evenly distributed on the DMAB molecule (Fig. 4(a)), whereas a highly asymmetric charge density distribution (Fig. 4(b)) was found in the case of the Au tip–Ag substrate geometry.

For a molecule placed in an inhomogeneous electromagnetic field, the induced dipole moment of the molecule is given by the equation[23]

$$\mu_\alpha = \alpha_{\alpha\beta}E_\beta + \frac{1}{3}A_{\alpha\beta\gamma}\frac{\partial E_\beta}{\partial r} + \cdots, \tag{1}$$

where {α, β, γ} are coordinates in the Cartesian coordinate system and the tensor convention in repeated subscripts is applied. $\alpha_{\alpha\beta}$ and $A_{\alpha\beta\gamma}$ are respectively the dipole and quadrupole polarizabilities and are given by the expressions

$$\alpha_{\alpha\beta} = \sum_j H(\omega)(\langle i|\mu_\alpha|j\rangle\langle j|\mu_\beta|f\rangle)/\hbar, \tag{2}$$
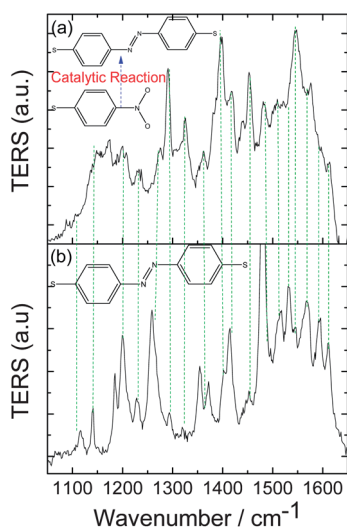
Fig. 3 Comparison between (a) the TER spectrum of DMAB dimerized from the 4NBT adsorbed on a gold film and (b) the genetic TER spectrum of DMAB adsorbed on a gold film.
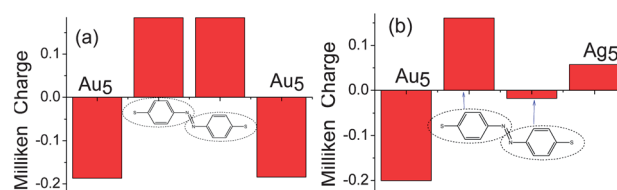
Fig. 4 Charge distributions in (a) Au$_5$–DMAB–Au$_5$ and (b) Au$_5$–DMAB–Ag$_5$ configurations.

$$A_{\alpha\beta\gamma} = \sum_j H(\omega)(\langle i|\mu_\alpha|j\rangle\langle j|\theta_{\beta\gamma}|f\rangle)/\hbar, \tag{3}$$

where $H(\omega) = \omega_{ji}^2/(\omega_{ji} - \omega^2)$. μ_α and $\theta_{\beta\gamma}$ are the molecular electric dipole and quadrupole operators. i and f refer to the initial and final states of the system. For Raman spectroscopy, the vibrational coordinate of the molecule should be considered. Therefore α and A should be understood to represent $\partial\alpha/\partial Q$ and $\partial A/\partial Q$, where Q is a normal coordinate to the vibration of the molecule.[23]

The two terms in eqn (1) give rise to the dipole Raman modes and electric field gradient multipolar Raman modes respectively. The ratio between contributions from the higher order terms to the dipole term can be estimated as

$$\left(\frac{1}{3}A_{\alpha\beta\gamma}\frac{\partial E_\beta}{\partial r}\right)\bigg/(\alpha_{\alpha\beta}E_\beta) \approx \frac{1}{3} \times \frac{A_{\alpha\beta\gamma}}{\alpha_{\alpha\beta}} \times \frac{\partial E_\beta/\partial r}{E_\beta}, \tag{4}$$

where $A_{\alpha\beta\gamma}/\alpha_{\alpha\beta}$ has the unit and magnitude of a molecular dimension. For molecules excited by electromagnetic waves in a vacuum, the electric field gradient term $\partial E_\beta/\partial r$ computes to $i(2\pi/\lambda)E_\beta$. Therefore eqn (4) will be of the order of the ratio of molecular dimension to excitation wavelength, which is approximately 10^{-3}. On the other hand, in space close to a metal surface, the jellium approximation of Feibelman[24] states that the electric field varies by nearly its full amplitude over a distance of 0.2 nm, which means the field gradient term is approximately $\lambda/0.2$ nm and that eqn (4) will now compute to unity, indicating that the induced quadrupole term cannot be ignored near metal surfaces.

For the Au tip–Au substrate geometry, the symmetric charge distribution on the DMAB molecule means that the dipole polarizability in eqn (1) is negligible compared to the quadrupole polarizability. The electric field gradient effects, which resulted from the highly asymmetric geometry of the sharp Au tip and the substrate, result in the activation of IR-active bu modes with strong enhancement.[14,16] On the other hand, for the Au tip–Ag substrate geometry, the asymmetric charge distribution on the DMAB molecule leads to a large dipole polarizability and renders the quadrupole term negligible. As a result, there was no activation of IR-active modes observed experimentally. Further, the fact that the dipole polarizability is predominant for the Ag substrate but negligible for the Au substrate can also explain the experimental observation that the TERS signals with the Ag substrate (Fig. 2(a) in ref. 9a) are much stronger than those with the Au substrate (Fig. 1(c)). In short, for a symmetric molecule in the tip–substrate nanogap with the same material, the quadrupole polarizability in eqn (1) dominates and we

observed the second order electric field gradient enhanced quadrupole Raman modes. In the case of the tip–substrate nanogap with different materials, the dipolar term dominates. What we observed in TER spectra was the first order electric field enhanced dipole Raman modes.

Moreover, the qualitative relationship between the Fermi levels of the Au tip, the Au substrate and orbital energy levels of DMAB molecules can be obtained both before (Fig. 5(a)) and after (Fig. 5(b)) charge transferring from the tip or the substrate to DMAB molecules. After the charge transfer, it was found that the HOMO level dropped while the Fermi levels of the tip and the substrate rose. Fig. 5(c) illustrates the situation when an external voltage is applied so that the Fermi level of the tip (or the substrate) is raised to be higher than the LUMO level. As a result, electrons will transfer from the gold tip (or the substrate) to DMAB and then from DMAB to the gold substrate (or tip). In comparison, when the applied voltage is not high enough, the electrons can only transfer from the gold tip or the substrate to DMAB *via* electron tunneling. On the other hand, for the Au tip–DMAB–Ag substrate geometry, the Fermi levels of the Au tip, the Ag substrate and orbital energy levels of DMAB before (Fig. 5(d)) and after (Fig. 5(e)) the charge transferring were also calculated. Fermi levels of the Au tip and the Ag substrate are shifted close to the LUMO level as a result of electron transfer. In addition, when a low external voltage is applied to this system, the Fermi level of the Au tip or the Ag substrate will be raised to be higher than the LUMO level (Fig. 5(f)) and results in an energy favorable electron transfer from the Au tip to DMAB to the Ag substrate, or the reverse transfer direction depending on the direction of the voltage applied. TER spectra obtained in this configuration involve electrons that have transferred through the molecule, therefore the Au tip–Ag substrate geometry generates stronger TERS signals with a lower requirement of the applied voltages compared to that required by the Au tip–Au substrate geometry.

As the above discussion suggests, there exists a compromise relation between obtaining strong TERS signals and activating the IR-active modes. In the Au tip–Ag substrate geometry, we obtained very strong TERS signals from Raman-active modes but the IR-active modes could not be excited since the dipole polarizability term dominates in eqn (1) and the Fermi energy levels of the metal tip and the substrate are closer to the LUMO level. On the other hand, for the geometry with the Au substrate, both the Raman- and IR-active modes are excited but the signal intensities were low. It should be noted that the symmetry properties of the charge distribution on molecules also change the values of dipole and quadrupole polarizabilities in eqn (1) and determine the predominant term between the two. In addition, the above theoretical calculations also explained the reason why the IR-active modes of DMAB were not observed in the TERS spectra measured by the Au tip–Ag substrate system.[10]

In summary, the plasmon-driven catalytic reactions for molecules adsorbed on a Au film have been investigated using HV-TERS. TER spectra revealed that the electric field gradient results in a strong enhancement of IR-active modes of DMAB, as well as Raman active modes. The simultaneous observation of Raman-active and IR-active modes of DMAB in HV-TER spectra provided convincing spectral information for ultrasensitive chemical analysis. Theoretical calculations strongly supported experimental observation.

Acknowledgements

Notes and references

1 Y. Fang, Y. Li, H. Xu and M. Sun, *Langmuir*, 2010, **26**, 7737.

2 H. Zhu, X. Ke, X. Yang, S. Sarina and H. Liu, *Angew. Chem., Int. Ed.*, 2010, **49**, 9657.

3 Y. Huang, H. Zhu, G. Liu, D. Wu, B. Ren and Z. Tian, *J. Am. Chem. Soc.*, 2010, **132**, 9244.

4 P. Christopher, H. Xin and S. Linic, *Nat. Chem.*, 2011, **3**, 467.

5 (*a*) B. Dong, Y. Fang, X. Chen, H. Xu and M. Sun, *Langmuir*, 2011, **27**, 10677; (*b*) L. Kang, P. Xu, B. Zhang, H. Tsai, X. Han and H.-L. Wang, *Chem. Commun.*, 2013, **49**, 3389–3391.

6 S. Gao, K. Ueno and H. Misawa, *Acc. Chem. Res.*, 2011, **44**, 251.

7 V. Joseph, C. Engelbrekt, J. Zhang, U. Gernert, J. Ulstrup and J. Kneipp, *Angew. Chem., Int. Ed.*, 2012, **51**, 7592.

8 S. Mukherjee, F. Libisch, N. Large, O. Neumann, L. V. Brown, J. Chen, J. B. Lassiter, E. A. Carter, P. Nordlander and N. J. Halas, *Nano Lett.*, 2013, **13**, 240.

9 (*a*) M. Sun, Z. Zhang, H. Zheng and H. Xu, *Sci. Rep.*, 2012, **2**, 647; (*b*) Z. Zhang, L. Chen, M. T. Sun, P. Ruan, H. Zheng and H. Xu, *Nanoscale*, 2013, **5**, 3249.
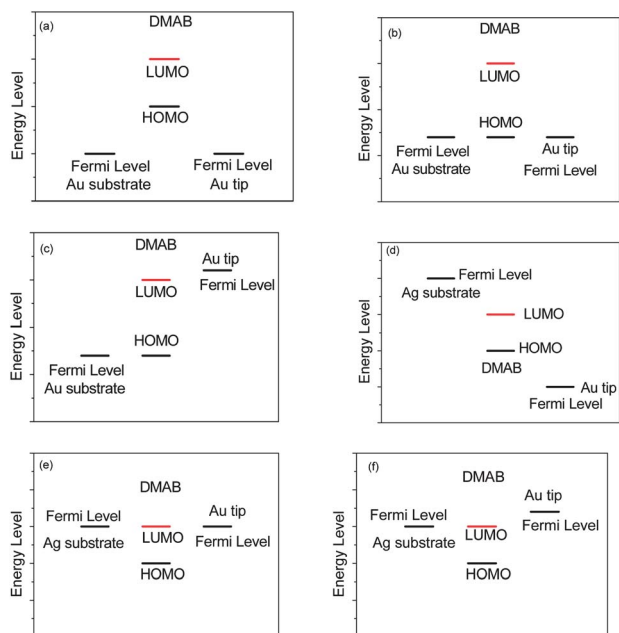
Fig. 5 The relationship between the Fermi level of metals and orbital energy levels of DMAB.

10 M. van Schrojenstein Lantman, T. Deckert-Gaudig, A. J. G. Mank, V. Deckert and B. M. Weckhuysen, *Nat. Nanotechnol.*, 2012, **7**, 583.

11 H. Kim, K. M. Kosuda, R. P. Van Duyne and P. C. Stair, *Chem. Soc. Rev.*, 2010, **39**, 4820.

12 M. Sun and H. Xu, *Small*, 2012, **8**, 2777.

13 M. Moskovits and D. P. DiLella, *J. Chem. Phys.*, 1980, **73**, 6068.

14 E. J. Ayars, H. D. Hallen and C. L. Jahncke, *Phys. Rev. Lett.*, 2000, **85**, 4180.

15 E. Fermi, *Z. Phys.*, 1931, **71**, 250.

16 M. Sun, Y. Fang, Z. Zhang and H. Xu, *Phys. Rev. E: Stat., Nonlinear, Soft Matter Phys.*, 2013, **87**, 020401(R).

17 B. T. Darling and D. M. Dennison, *Phys. Rev.*, 1940, **57**, 128.

18 Y. Li, P. Wang, Z. Zhang, Y. Li, F. Ma and M. T. Sun, *RSC Adv.*, 2012, **2**, 12160.

19 Z. Zhang, L. Chen, M. T. Sun, H. X. Xu, *Adv. Opt. Mater.*, submitted.

20 B. Ren, G. Picardi and B. Pettinger, *Rev. Sci. Instrum.*, 2004, **75**, 837.

21 B. Dong, Y. Fang, L. Xia, H. Xu and M. Sun, *J. Raman Spectrosc.*, 2011, **42**, 1205.

22 *Gaussian 09, Revision A.02*, Gaussian, Inc., Wallingford CT, 2009.

23 A. D. Buckingham, *Adv. Chem. Phys.*, 1967, **12**, 107.

24 P. J. Feibelman, *Phys. Rev. B: Solid State*, 1975, **12**, 1319.